Published in "EPL (Europhysics Letters) 119 (5): 57007, 2017"
which should be cited to refer to this work.

# Pressure-driven insulator-metal transition in cubic phase $UO_2$

Li Huang[1], Yilin Wang[2] and Philipp Werner[3]

[1] *Science and Technology on Surface Physics and Chemistry Laboratory - P.O. Box 9-35, Mianyang 621908, China*
[2] *Condensed Matter Physics and Materials Science Division, Brookhaven National Laboratory Upton, NY 11973, USA*
[3] *Department of Physics, University of Fribourg - 1700 Fribourg, Switzerland*

PACS 71.30.+h – Metal-insulator transitions and other electronic transitions
PACS 71.27.+a – Strongly correlated electron systems; heavy fermions
PACS 71.20.-b – Electron density of states and band structure of crystalline solids

**Abstract** – Understanding the electronic properties of actinide oxides under pressure poses a great challenge for experimental and theoretical studies. Here, we investigate the electronic structure of cubic phase uranium dioxide at different volumes using a combination of density functional theory and dynamical mean-field theory. The *ab initio* calculations predict an orbital-selective insulator-metal transition at a moderate pressure of ∼45 GPa. At this pressure the uranium's $5f_{5/2}$ state becomes metallic, while the $5f_{7/2}$ state remains insulating up to about 60 GPa. In the metallic state, we observe a rapid decrease of the $5f$ occupation and total angular momentum with pressure. Simultaneously, the so-called "Zhang-Rice state", which is of predominantly $5f_{5/2}$ character, quickly disappears after the transition into the metallic phase.



**Introduction.** – Over the past decades, actinide materials including pure elements, hydrides, oxides, carbides, and nitrides have been extensively studied with numerous experimental and theoretical tools, due to their fundamental importance in the nuclear energy industry and military technology [1,2]. Even though great progress has been made, many problems and puzzles still remain. Of particular interest are the electronic structures of these actinide materials under extreme conditions (for example high pressure and high temperature in a reactor environment or a reactor accident) [3,4].

Experimentally, it has been observed that under pressure many actinide materials may undergo a series of structural phase transitions, such as the cubic to orthorhombic phase transitions occurring in some actinide dioxides [5], and the three successive phase transitions in Am [6]. The explanation of these complex phase transitions requires an accurate description of the properties of the $5f$ electrons over a wide range of pressures. It is well known that the $5f$ electrons, which play a pivotal role in determining the key physical and chemical properties of the actinide materials, react sensitively to changes in the surrounding environment [1,2]. So, it is natural to expect that the $5f$ electronic structures of actinide materials will be modified and some exotic effects and phenomena may emerge when an external pressure is applied. Up to now, only a few experiments and calculations have been conducted to explore the high-pressure properties of actinide materials, and most of these efforts were devoted to study their structural phase transitions and phase instabilities [4–7]. As a consequence, the high-pressure electronic structures of actinide materials are poorly understood. Motivated by these facts, we employ a state-of-the-art first-principles approach to shed new light onto the pressure-driven electronic transitions in uranium dioxide, which is one of the most important nuclear fuels.

Under ambient pressure, stoichiometric $UO_2$ is in a fluorite ($CaF_2$) structure. A transition from the cubic phase to orthorhombic cotunnite structure in the range of 42–69 GPa [5] was already determined by high-precision X-ray diffraction experiments. The ground state of $UO_2$ is an antiferromagnetic Mott insulator with a sizeable band gap of ∼2.1 eV [8]. To study the electronic structure of $UO_2$, many traditional first-principles approaches have been employed, such as the local density approximation (LDA) (or generalized gradient approximation (GGA)) plus Hubbard $U$ approach [9–13], the hybrid functional method [14], and the self-interaction corrected local spin-density approximation (SIC-LSDA) [15]. However, none of the above methods can provide a satisfactory description of $UO_2$ over a wide range of conditions. For instance, even though the band gap at ambient pressure is

reproduced correctly, the phase transition pressures predicted by the LDA + $U$ and GGA + $U$ methods are 7.8 [9] and 20 GPa [13], respectively, and thus much lower than the experimental value. This discrepancy is likely due to the incorrect treatment of the multiple metastable states of $UO_2$ [11]. In addition, the changes of the electronic structure, especially the evolution of the Mott gap of $UO_2$ under pressure, is still an open and debated question [3].

Since $UO_2$ is a correlated electron material, the strong Coulomb interaction among uranium's $5f$ electrons have to be considered in the calculations in order to obtain a correct description of its electronic structure [16,17]. The density functional theory plus single-site dynamical mean-field theory (dubbed DFT + DMFT) method [18,19], which combines the first-principles aspect of DFT with a many-body treatment of local interaction effects, captures the essence of electronic correlations in realistic materials. Based on the assumption of a local electronic self-energy, the DFT + DMFT method is currently the most powerful established tool to study strongly correlated systems, and has been widely employed to investigate the electronic structures and structural phase transitions of actinide materials (including metal elements, oxides, nitrides, etc.) [16,17,20–26]. In this paper, we employ the charge fully self-consistent DFT + DMFT method to explore the electronic structures of cubic phase $UO_2$ under various pressures. We predict that an orbital-selective insulator-metal transition will occur around 45 GPa. We also find that the pressure effect will lead to not only a redistribution of the $5f$ electrons and an associated decline of total angular momentum, but also a disappearance of the peak of predominantly U-$5f$ character which is located in the energy range between $-2.0$ eV and $-1.0$ eV.

**Methods.** – The DFT + DMFT calculations were performed by using the `EDMFTF` package which has been developed by Haule *et al.* [27] on top of the full-potential linearized augmented plane-wave code `WIEN2k` [28]. Usually 40 DFT + DMFT iterations are sufficient to obtain a well-converged charge density $\rho$ and total energy $E$. The cutoff parameter $R_{\mathrm{MT}}K_{\mathrm{MAX}}$ was set to 7.0 and a $12\times12\times12$ uniform $k$-mesh was adopted for the Brillouin zone integration. The spin-orbit coupling was included in a second variational way in the DFT calculation. As for the Coulomb interaction (which is only taken into considerations for the U-$5f$ orbitals), we built a four-fermion interaction matrix which is parameterized by the Slater integrals $F^k$. For the $5f$ electronic systems, these Slater integrals approximately satisfy the following relations [29]:

$$U = F^0, \quad J = \frac{2}{45}F^2 + \frac{1}{33}F^4 + \frac{50}{1287}F^6, \tag{1}$$

and

$$F^4 = \frac{451}{675}F^2, \quad F^6 = \frac{1001}{2025}F^2, \tag{2}$$

where $U$ and $J$ are the Coulomb interaction strength and Hund's exchange parameter, respectively. We chose $U = 6.0$ eV and $J = 0.6$ eV in our calculations, in accord with the previous DFT + DMFT calculations [16]. For the double counting term, we used the fully localized limit scheme [30], which is commonly used in DFT + $U$ or DFT + DMFT calculations for correlated insulators [9–13]. All of the calculations were carried out at the inverse temperature $\beta = 100\,\mathrm{eV}^{-1}$ ($T \approx 116$ K), which is much higher than the experimental Néel temperature ($T_N = 30.8$ K) [2]. For this reason, we only conducted paramagnetic calculations. The hybridization expansion version of the continuous-time quantum Monte Carlo (dubbed CT-HYB) method [31–34] was used as the quantum impurity solver. For each DMFT iteration, $3\times10^8$ Monte Carlo updates were performed to reach sufficiently high accuracy. We utilized the maximum entropy method [35] to do the analytical continuation to extract the real-frequency self-energy $\Sigma(\omega)$ from the Matsubara self-energy $\Sigma(i\omega_n)$. $\Sigma(\omega)$ is an essential input for the calculation of the density of states $A(\omega)$, momentum-resolved spectral functions $A(\mathbf{k},\omega)$, and quasiparticle weight $Z$ [19].

Table 1: Calculated and experimental bulk properties and band gaps for cubic phase $UO_2$. Here $a_0$ denotes the lattice constant (unit: Å), $B$ the bulk modulus (unit: GPa), $E_{\mathrm{gap}}$ the band gap (unit: eV).

| Method | $a_0$ | $B$ | $E_{\mathrm{gap}}$ | Reference |
|---|---|---|---|---|
| DFT + DMFT | 5.565 | 211.2 | 2.1 | This work |
| DFT + $U$ | 5.540 | 191.6 | 2.2 | Ref. [10] |
| DFT + $U$ | 5.449 | 222.4 | 2.3 | Ref. [12] |
| SIC-LSDA | 5.400 | 219.0 | 0.0 | Ref. [15] |
| Hybrid functional | 5.463 | 218.0 | 2.4 | Ref. [14] |
| Experiments | 5.473 | 207.2 | 2.1 | Refs. [5,8] |

**Results.** – *Bulk properties at ambient pressure.* We firstly calculate the bulk properties of cubic phase $UO_2$ at ambient pressure to benchmark the accuracy of the present DFT + DMFT approach. We use the equation of states proposed by Teter *et al.* [36] to fit the $E$-$V$ curve, and then extract useful data. The calculated results are summarized in table 1. Other theoretical and experimental values, if available, are collected and listed as well. The obtained equilibrium lattice parameter $a_0$ is slightly overestimated, while the bulk modulus $B$ agrees with the experimental value quite well [5]. The small deviations ($\sim$1.7% for $a_0$ and $\sim$1.9% for $B$) prove that the computational parameters used in the present work are quite reasonable.

*Electronic structure at ambient pressure.* The electronic structure of $UO_2$ at ambient pressure is shown in fig. 1. We can see that the DFT + spin-orbit coupling (SOC) method fails to reproduce the insulating nature of $UO_2$, and leads to a metallic state (see fig. 1(a)). Thus, considering the SOC effect alone is not sufficient for a proper description of the electronic structure of $UO_2$.

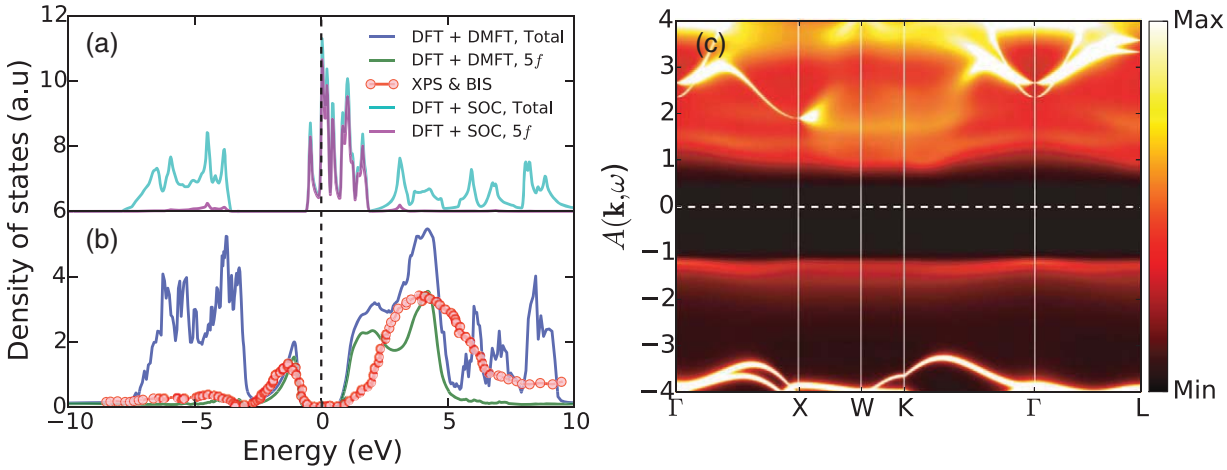


Fig. 1: (Color online) Electronic structure of cubic $UO_2$ at ambient pressure. (a) Total and $5f$ partial density of states obtained by the DFT + SOC method. (b) Total and $5f$ partial density of states obtained by the DFT + DMFT method. The XPS and BIS experimental data (denoted by red filled circles) [8] are shown for comparison. Note that panels (a) and (b) share the same legend. (c) The momentum-resolved spectral function $A(\mathbf{k},\omega)$ obtained by the DFT + DMFT method.



In fig. 1(b) and (c), the density of states $A(\omega)$ and momentum-resolved spectral functions $A(\mathbf{k},\omega)$ obtained by the DFT + DMFT approach are shown, together with the available XPS and BIS experimental data [8]. From the calculated results, we can conclude that: i) The energy gap is about 2.1 eV, which is consistent with the experimental value (see table 1) [8]. Note that the band gap is very sensitive to the chosen values of $U$. If $U = 8.0$ eV (or 4.5 eV), the calculated band gap is about 2.6 eV (or 1.5 eV). ii) Since the energy gap is mainly associated with $5f \rightarrow 5f$ transitions, uranium dioxide is a Mott insulator, which is consistent with the experiments [37,38] and most of the first-principles results [14]. iii) Between $-2.0$ eV and $-1.0$ eV, there exists an isolated peak which is predominantly of U-$5f$ and O-$2p$ character. Its position and spectral weight agree quite well with the XPS experiments [8,37]. Recently, Yin *et al.* [16] suggested that this low-energy resonance can be viewed as a generalized Zhang-Rice state ("ZRS") [39]. According to their interpretation, the many-body ground state of the $UO_2$ $5f^2$ electronic configuration is a $\Gamma_5$ triplet, and there must be a local magnetic moment which will couple with the O-$2p$'s hole induced by the photoemission process. Whether or not this peak can indeed be associated with Zhang-Rice physics is still being debated, but in the following we will use "ZRS" to denote this peak for the sake of simplicity.

*Pressure-driven insulator-metal transition.* Next, we concentrate on the pressure-driven electronic structure transition in cubic phase $UO_2$. We decrease the lattice constant $a_0$ to mimic the increase of external pressure, while the crystal structure and the atomic coordinates are kept fixed. The evolution of the density of states with volume, as predicted by DFT + DMFT, is shown in fig. 2(a). As the volume (pressure) is decreased (increased), dramatic changes are observed in the density of states. The band gap shrinks monotonously, and disappears suddenly at $V/V_0 = 0.85$, which marks an insulator-metal transition. The critical transition pressure $P_c$ is about 45 GPa according to the experimental $P$-$V$ curve [5]. When $P > P_c$, the quasi-particle peak grows quickly, which implies an enhancement of metallicity. The peak associated with the "ZRS" is also very sensitive to the volume collapse. Even though no strong shift of the "ZRS" peak to lower energies is apparent, which roughly agrees with previous DFT + DMFT calculations [16], there is a substantial transfer of spectral weight to the quasi-particle peak. At $V/V_0 = 0.80$ (corresponding to $P \approx 65$ GPa) [5], the "ZRS" peak is almost smeared out. The multiple peaks located in the energy range from $-12$ to $-3$ eV and from 1 to 10 eV are predominantly of O-$2p$ and U-$6d$ characters [37], respectively. They are strongly hybridized with the lower and upper Hubbard bands of the U-$5f$ orbitals which are approximately located at $-5$ to $-4$ eV and 1 to 6 eV, respectively [16]. These occupied ligand bands are also shifted outward and broaden under pressure. We further calculate the momentum-dependent spectral functions $A(\mathbf{k},\omega)$ at various volumes in order to gain a better understanding of the evolutions of the band gap and the "ZRS". Selected results are visualized in fig. 2(c1)–(c5). These plots reveal the same insulator-metal transition scenario as already shown in fig. 2(a). From (c1) to (c3), the Mott gap is reduced from a finite value (2.1 eV) to zero, and the "ZRS" feature is slightly shifted toward the Fermi level. In panel (c3), where $V/V_0 = 0.85$, the quasi-particle peak appears, while the "ZRS" peak still persists. From (c3) to (c5), the "ZRS" peak is rapidly smeared out and, on the contrary, the weight of the quasi-particle peak is substantially enhanced.

Due to the SOC effect in heavy elements, the U-$5f$ orbitals are split into two components: $5f_{5/2}$ and $5f_{7/2}$

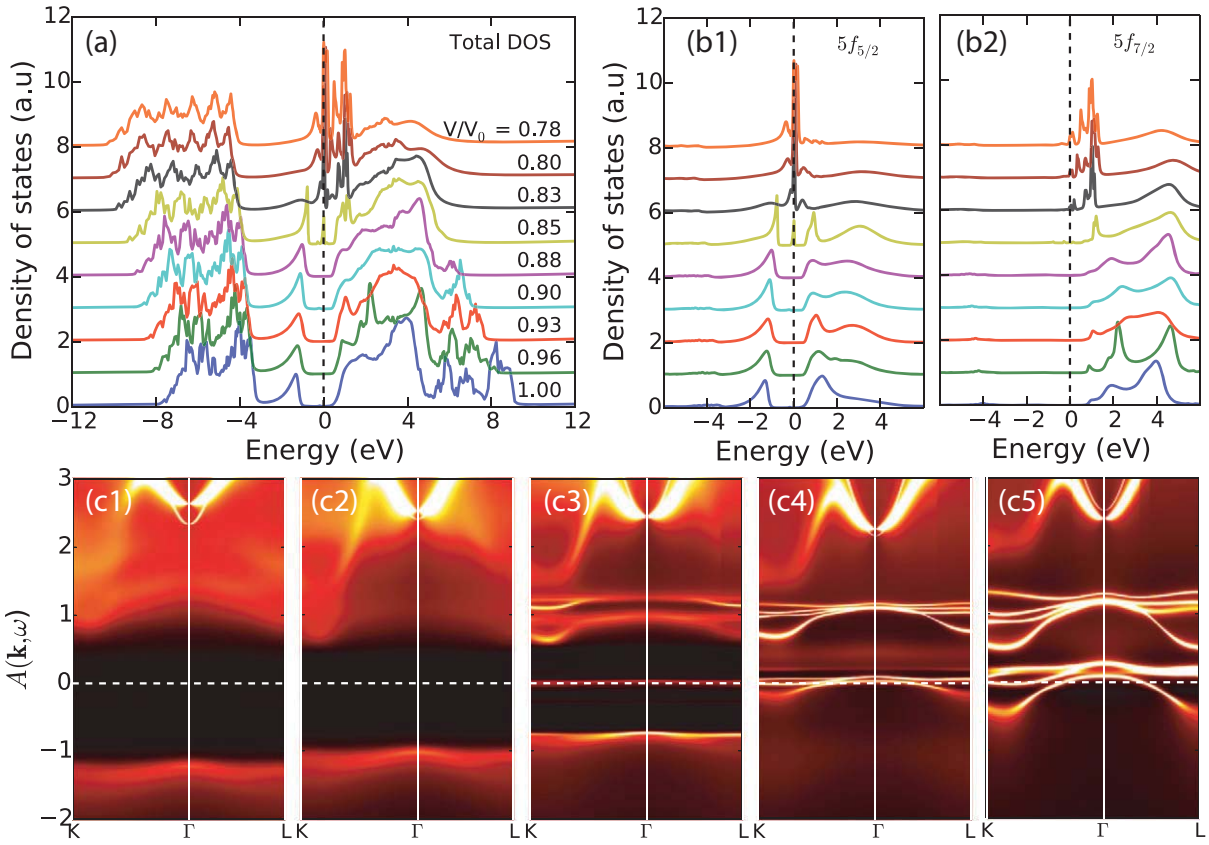


Fig. 2: (Color online) Evolution of the electronic structure of cubic $UO_2$ under pressure calculated by the DFT + DMFT method. (a) Total density of states $A(\omega)$. (b1) The $5f_{5/2}$ partial density of states $A_{5f_{5/2}}(\omega)$. (b2) The $5f_{7/2}$ partial density of states $A_{5f_{7/2}}(\omega)$. (c1)–(c5) The momentum-resolved spectral functions $A(\mathbf{k},\omega)$ for $V/V_0 = 1.00$, 0.90, 0.85, 0.83, and 0.78, respectively. Notice that there exists a sharp quasi-particle peak sitting at the Fermi level in panel (c3).

states (here we ignore the crystal field splitting for simplicity) [1]. It is interesting to study the partial density of states $A_{5f_{5/2}}(\omega)$ and $A_{5f_{7/2}}(\omega)$ under pressure. The calculated results are shown in fig. 2(b1) and (b2), respectively. If one compares the $5f_{5/2}$ partial density of states in fig. 2(b1) with the total density of states in fig. 2(a), one can easily recognize that both the band gap and the "ZRS" peak are associated primarily with the $5f_{5/2}$ state. In fig. 2(b1), one can observe again how a quasi-particle peak grows at the Fermi level and the "ZRS" peak fades away when $V/V_0 \leq 0.85$. Thus, we consider that the $5f_{5/2}$ state is responsible for the pressure-driven insulator-metal transition and the associated disappearance of the "ZRS" peak in cubic phase $UO_2$. As for the $5f_{7/2}$ state, most of the spectral weight is well above the Fermi level. Remarkably, even when $V/V_0 = 0.85$ (the approximate transition point for the $5f_{5/2}$ state), the spectral weight for the $5f_{7/2}$ state at the Fermi level remains zero. Only for $V/V_0 \leq 0.83$, the $5f_{7/2}$ state becomes metallic. In other words, the insulator-metal transitions for the two states do not occur simultaneously, and there is a sizable volume or pressure regime (*i.e.*, $V/V_0 \in [0.83, 0.85]$ or $P \in [45, 60]$ GPa [5]) in which the $5f_{5/2}$ state is metallic while the $5f_{7/2}$ state remains insulating. According to our calculations, the insulator-metal transition in cubic phase $UO_2$ is therefore orbital-selective [40,41].

In addition to the total (partial) density of states, we can use the real-frequency self-energy $\Sigma(\omega)$ and quasi-particle weight $Z$ to identify the insulator-metal transition. We can evaluate $Z$ via the following equation [18]:

$$Z^{-1} = 1 - \frac{\partial}{\partial\omega}\mathrm{Re}\Sigma(\omega)\Big|_{\omega=0}. \qquad (3)$$

The obtained orbital-resolved $\Sigma(\omega)$ and $Z$ are shown in fig. 3(a) and (b), respectively. For $V/V_0 > 0.85$, the $\mathrm{Re}\Sigma_{5f_{5/2}}(\omega)$ display a clear insulating characteristic, and the corresponding $Z \approx 0$. For $V/V_0 \leq 0.85$, the $\mathrm{Re}\Sigma_{5f_{5/2}}(\omega)$ exhibits a quasi-linear behavior in the vicinity of $\omega = 0$ and $Z > 0$, which is a signature of a metallic state. Thus, based on the self-energy data, we can conclude that the insulator-metal transition for the $5f_{5/2}$ state occurs near $V/V_0 = 0.85$. On the other hand, between $-2$ eV and $-1$ eV, where the "ZRS" peak usually lives, we do not observe any special features in $\mathrm{Re}\Sigma_{5f_{5/2}}(\omega)$ which is roughly consistent with the previous DFT + DMFT calculations [16]. Since at low temperature, the quantity $|\beta G(\beta/2)|$ is proportional to $A(\omega = 0)$, it is often used by the DMFT community to locate the

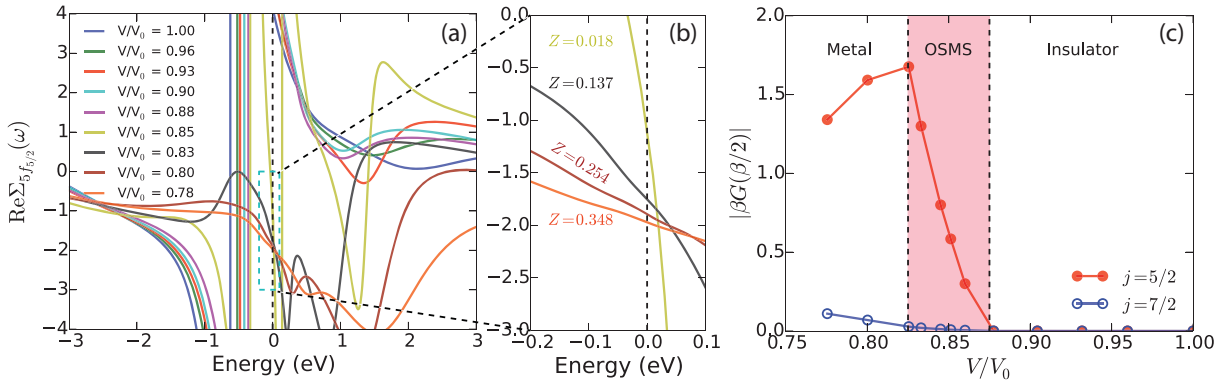


Fig. 3: (Color online) (a) Real part of the local self-energy $\mathrm{Re}\Sigma(\omega)$ for various volumes. Only the $5f_{5/2}$ components are shown. (b) Zoom of the area enclosed by dashed cyan lines in panel (a). Here $Z$ denotes the quasi-particle weight, which is calculated via eq. (3). (c) $|\beta G(\beta/2)|$ for the $5f_{5/2}$ and $5f_{7/2}$ states as a function of volume. $\beta = T^{-1}$ and $G$ is the imaginary-time Green's function. In the pink region, the material is in an orbital-selective Mott state (OSMS).

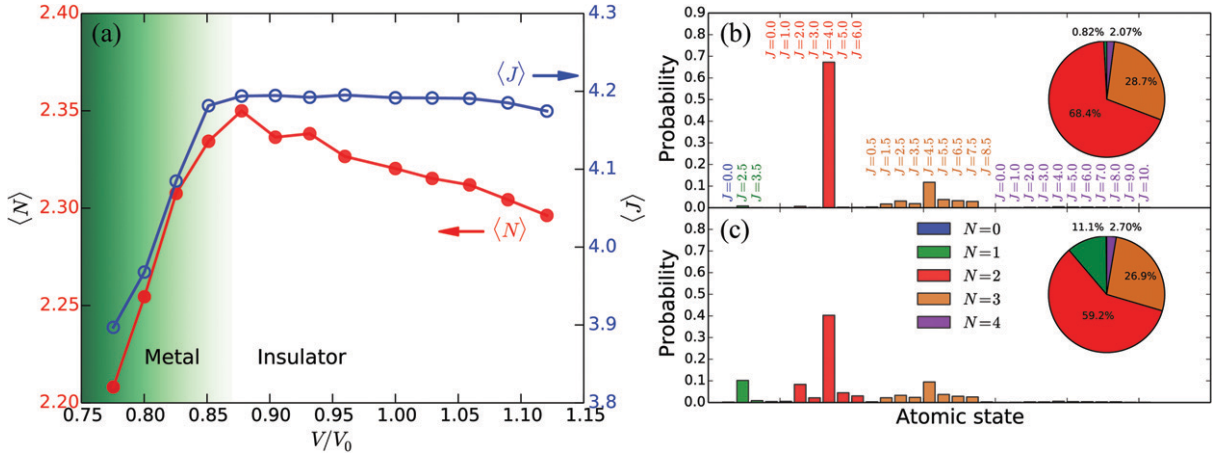


Fig. 4: (Color online) (a) The average $5f$ electron occupancy $N_{5f} = \langle N \rangle$ (left $y$-axis) and total angular momentum $\langle J \rangle$ (right $y$-axis) for various volumes. (b), (c): valence state histograms at $V/V_0 = 1.00$ (insulating region) and 0.78 (metallic region), respectively. The pie diagrams show the distributions of atomic eigenstates with respect to $N$. The atomic eigenstate probability for the $|N = 0\rangle$ state is too small to be visible.



metal-insulator transition. Here we calculate it for the $5f_{5/2}$ and $5f_{7/2}$ states, and use it to support the orbital-selective insulator-metal transition scenario. As is clearly seen in fig. 3(c), the orbital-selective Mott phase (OSMP) lies roughly between $V/V_0 = 0.83$ and $V/V_0 = 0.87$. When $V/V_0 < 0.83$, both states exhibit correlated metallic behaviors. However, they are insulating when $V/V_0 > 0.87$.

*$5f$ occupancies and valence state histograms.* The nominal $5f$ occupation for $UO_2$ is 2. However, due to the strong hybridization between the U-$5f$ and O-$2p$ bands [37], the actual $5f$ occupation is slightly larger than 2. We analyzed the connection between the average $5f$ orbital occupancy $N_{5f}$ and the volume collapse $V/V_0$ (see fig. 4(a)). Under compression, $N_{5f}$ first increases steadily, and then decreases sharply. This behavior can be easily understood as follows: In the insulating phase, the $5f$ electrons are localized and the moderate changes in $N_{5f}$ are due to the hybridization effect with the O-$2p$ bands. In the metallic phase, the $5f$ electrons become itinerant which allows them to hop from the $5f_{5/2}$ state to the $5f_{7/2}$ state, the O-$2p$ and U-$6d$ orbitals easily. As a result, one finally observes an abrupt decline of $N_{5f}$ after the insulator-metal transition.

The valence state histogram, which measures the probability to find a $5f$ electron in a given atomic eigenstate, can provide additional information about the nature of the $5f$ electrons [21,32]. Representative valence state histograms for $V/V_0 = 1.00$ (insulating phase) and 0.78 (metallic phase) are plotted in fig. 4(b) and (c), respectively. In the insulating phase, the dominant atomic eigenstates have occupancy $N = 2$ and 3. The other atomic eigenstates only have negligible weights. In the metallic phase, even though the $|N = 2\rangle$ and $|N = 3\rangle$ atomic eigenstates still remain dominant, the probabilities for the $|N = 1\rangle$ atomic eigenstates increase substantially. So, the change in the

valence state histogram is consistent with the rapid decrease of $N_{5f}$. We further calculated the effective total angular momentum $\langle J\rangle$ using $\langle J\rangle = \sum_\Gamma p_\Gamma J_\Gamma$ where $p_\Gamma$ is the probability for the atomic eigenstate $\Gamma$. In the insulating phase, $\langle J\rangle$ is hardly affected by the volume compression, while in the metallic phase it decreases steeply (see fig. 4(a)). We note that the reduction of the total angular momentum under pressure is rather similar to the spin state crossover observed in some transition metal oxides [42,43], so it is likely the driving force behind the "melting" of the "ZRS" peak.

**Discussion and conclusion.** – The calculations presented in this paper ignore the structural phase transition. In fact, the structural phase transition from cubic to orthorhombic begins at $V/V_0 = 0.87$, and continues beyond $V/V_0 = 0.81$. The transition zone extends at least up to 69 GPa [5]. Since the electronic transition apparently can occur without any change in crystal structure and the $P_c$ for it is very close to the one for the experimentally observed structural phase transition, we believe that the structural phase transition in $UO_2$ is driven by the electronic transition, which involves a localization-delocalization process of the U-5$f$ electrons. Previous theoretical research using the LDA + $U$ method predicted that the orthorhombic structure is an insulator, and the metallization pressure for it is in the range of 226–294 GPa [9]. On the other hand, the SIC-LSDA approach predicted that the cubic $UO_2$ is on the verge of an insulator-metal transition at ambient pressure [3]. Both predictions are inconsistent with ours and it would thus be very interesting to test them experimentally.

In summary, we propose that the insulator-metal transition in cubic $UO_2$ occurs at $P_c \approx 45$ GPa and is of the orbital-selective type [40,41]. There are two successive transitions for the $5f_{5/2}$ and $5f_{7/2}$ states, respectively. The "ZRS" peak is only prominent in the insulating phase. In the metallic state, it quickly fades away with increasing pressure. At the same time, in the metallic phase, the pressure effect leads to a rapid decrease of the 5$f$ occupancies and the total angular momentum. To our knowledge, this is the first study of the high-pressure electronic structure of actinide dioxide using a modern DFT + DMFT approach. Our findings imply that physical properties such as resistivity, optical conductivity, and the magnetic moment of $UO_2$ should change radically across the (electronically driven) structural phase transition. We further speculate that other actinide dioxides, such as $PaO_2$, $NpO_2$, $PuO_2$, $AmO_2$, and $CmO_2$ etc., should exhibit similar pressure-driven phenomena [14]. Thus, more high-pressure experiments and theoretical calculations are highly desired.

* * *

LH and PW acknowledge support from the Swiss National Science Foundation (Grant No. 200021_140648). LH is also supported by the National Science Foundation of China (Grant No. 11504340). Most of the DFT + DMFT calculations were performed on the UniFr cluster (in Fribourg University, Switzerland) and TianHe-1A (in the National Supercomputer Center in Tianjin, China).

REFERENCES

[1] Moore K. T. and van der Laan G., *Rev. Mod. Phys.*, **81** (2009) 235.
[2] Morss L., Edelstein N., Fuger J. and Katz J. (Editors), *The Chemistry of the Actinide and Transactinide Elements*, 4th edition, Vols. **1–6** (Springer, The Netherlands) 2011.
[3] Petit L., Szotek Z., Temmerman W., Stocks G. and Svane A., *J. Nucl. Mater.*, **451** (2014) 313.
[4] Benedict U., Dabos-Seignon S., Dancausse J., Gensini M., Gering G., Heathman S., Luo H., Olsen J. S., Gerward L. and Haire R., *J. Alloys Compd.*, **181** (1992) 1.
[5] Idiri M., Le Bihan T., Heathman S. and Rebizant J., *Phys. Rev. B*, **70** (2004) 014113.
[6] Heathman S., Haire R. G., Le Bihan T., Lindbaum A., Litfin K., Méresse Y. and Libotte H., *Phys. Rev. Lett.*, **85** (2000) 2961.
[7] Lindbaum A., Heathman S., Bihan T. L., Haire R. G., Idiri M. and Lander G. H., *J. Phys.: Condens. Matter*, **15** (2003) S2297.
[8] Baer Y. and Schoenes J., *Solid State Commun.*, **33** (1980) 885.
[9] Geng H. Y., Chen Y., Kaneta Y. and Kinoshita M., *Phys. Rev. B*, **75** (2007) 054111.
[10] Wang J., Ewing R. C. and Becker U., *Phys. Rev. B*, **88** (2013) 024109.
[11] Dorado B., Amadon B., Freyss M. and Bertolus M., *Phys. Rev. B*, **79** (2009) 235125.
[12] Wang B.-T., Zhang P., Lizárraga R., Di Marco I. and Eriksson O., *Phys. Rev. B*, **88** (2013) 104107.
[13] Yu J., Devanathan R. and Weber W. J., *J. Phys.: Condens. Matter*, **21** (2009) 435401.
[14] Wen X.-D., Martin R. L., Henderson T. M. and Scuseria G. E., *Chem. Rev.*, **113** (2013) 1063.
[15] Petit L., Svane A., Szotek Z., Temmerman W. M. and Stocks G. M., *Phys. Rev. B*, **81** (2010) 045108.
[16] Yin Q., Kutepov A., Haule K., Kotliar G., Savrasov S. Y. and Pickett W. E., *Phys. Rev. B*, **84** (2011) 195111.
[17] Yin Q. and Savrasov S. Y., *Phys. Rev. Lett.*, **100** (2008) 225504.
[18] Georges A., Kotliar G., Krauth W. and Rozenberg M. J., *Rev. Mod. Phys.*, **68** (1996) 13.
[19] Kotliar G., Savrasov S. Y., Haule K., Oudovenko V. S., Parcollet O. and Marianetti C. A., *Rev. Mod. Phys.*, **78** (2006) 865.
[20] Haule K. and Kotliar G., *Nat. Phys.*, **5** (2009) 796.
[21] Shim J. H., Haule K. and Kotliar G., *Nature*, **446** (2007) 513.
[22] Zhu J.-X., Albers R. C., Haule K., Kotliar G. and Wills J. M., *Nat. Commun.*, **4** (2013) 3644.
[23] Kolorenč J. C. V., Shick A. B. and Lichtenstein A. I., *Phys. Rev. B*, **92** (2015) 085125.
[24] Amadon B., *J. Phys.: Condens. Matter*, **24** (2012) 075604.

[25] Dai X., Savrasov S. Y., Kotliar G., Migliori A., Ledbetter H. and Abrahams E., *Science*, **300** (2003) 953.
[26] Shick A. B., Havela L., Lichtenstein A. I. and Katsnelson M. I., *Sci. Rep.*, **5** (2015) 15429.
[27] Haule K., Yee C.-H. and Kim K., *Phys. Rev. B*, **81** (2010) 195107.
[28] Blaha P., Schwarz K., Madsen G., Kvasnicka D. and Luitz J., *WIEN2k, An Augmented Plane Wave + Local Orbitals Program for Calculating Crystal Properties* (Karlheinz Schwarz, Technische Universität Wien, Austria) 2001.
[29] Fujiwara T. and Korotin M., *Phys. Rev. B*, **59** (1999) 9903.
[30] Anisimov V. I., Aryasetiawan F. and Lichtenstein A. I., *J. Phys.: Condens. Matter*, **9** (1997) 767.
[31] Werner P., Comanac A., de' Medici L., Troyer M. and Millis A. J., *Phys. Rev. Lett.*, **97** (2006) 076405.
[32] Haule K., *Phys. Rev. B*, **75** (2007) 155113.
[33] Gull E., Millis A. J., Lichtenstein A. I., Rubtsov A. N., Troyer M. and Werner P., *Rev. Mod. Phys.*, **83** (2011) 349.
[34] Sémon P., Yee C.-H., Haule K. and Tremblay A.-M. S., *Phys. Rev. B*, **90** (2014) 075149.
[35] Jarrell M. and Gubernatis J., *Phys. Rep.*, **269** (1996) 133.
[36] Teter D. M., Gibbs G. V., Boisen M. B., Allan D. C. and Teter M. P., *Phys. Rev. B*, **52** (1995) 8064.
[37] Tobin J. G. and Yu S.-W., *Phys. Rev. Lett.*, **107** (2011) 167406.
[38] An Y. Q., Taylor A. J., Conradson S. D., Trugman S. A., Durakiewicz T. and Rodriguez G., *Phys. Rev. Lett.*, **106** (2011) 207402.
[39] Yin Q., Gordienko A., Wan X. and Savrasov S. Y., *Phys. Rev. Lett.*, **100** (2008) 066406.
[40] Koga A., Kawakami N., Rice T. M. and Sigrist M., *Phys. Rev. Lett.*, **92** (2004) 216402.
[41] Werner P. and Millis A. J., *Phys. Rev. Lett.*, **99** (2007) 126405.
[42] Kunes J., Lukoyanov A. V., Anisimov V. I., Scalettar R. T. and Pickett W. E., *Nat. Mater.*, **7** (2008) 198.
[43] Huang L., Wang Y. and Dai X., *Phys. Rev. B*, **85** (2012) 245110.